doi: 10.32131/jes.8.35

Journal of the Earth Simulator, Volume 8, November 2007, 35–44

Numerical Simulations of Turbulent Mixing in Eruption Clouds

Yujiro J. Suzuki[1]*, Takehiro Koyaguchi[2]

[1] *Institute for Research on Earth Evolution, Japan Agency for Marine-Earth Science and Technology, 3173-25, Showa-Machi, Yokohama 236-0001, Japan*
[2] *Earthquake Research Institute, University of Tokyo, 1-1-1, Yayoi, Bunkyo-ku, Tokyo 113-0032, Japan*

(Received June 18, 2007; Revised manuscript accepted July 24, 2007)

Abstract Eruption clouds in explosive volcanic eruptions are a kind of free boundary shear flow with very high Reynolds numbers ($Re > 10^8$), and their dynamics are governed by the entrainment of ambient air into eruption clouds by turbulent mixing and the density change of eruption clouds accompanied by turbulent mixing. We developed a numerical pseudo-gas model which correctly simulates turbulent mixing in and around eruption clouds by employing three-dimensional coordinates, a high-order accuracy scheme, and a fine grid size. Our model has successfully reproduced the quantitative features of turbulent mixing at high Reynolds numbers observed in laboratory experiments as well as fundamental features of the dynamics of eruption clouds, such as the generation of eruption columns and/or pyroclastic flows.

Keywords: volcanic eruption cloud, pseudo-gas model, turbulent mixing, volcanic hazard

1. Introduction

During explosive volcanic eruptions, a mixture of hot ash (pyroclasts) and volcanic gas is released from the volcanic vent into the atmosphere. Such events are characterized by the formation of eruption columns and/or pyroclastic flows. Generally, the ejecta (i.e., pyroclasts and volcanic gas) have an initial density of several times as large as the atmospheric density since it contains more than 90 wt% pyroclasts at the vent [1]. As the ejecta are mixed with ambient air, the density of the mixture drastically decreases and becomes less than the atmospheric density, because the entrained air expands by heating from the hot pyroclasts. When the ejecta entrain sufficient air to become buoyant, a large Plinian eruption column rises up to a height of several tens of kilometers as a turbulent plume. On the other hand, if the ejecta do not entrain sufficient air and their vertical velocity fall to zero before the eruption cloud becomes buoyant, a column collapse occurs and the heavy and hot cloud spreads radially as a pyroclastic flow. Thus dynamics of eruption clouds is governed by (1) the density change of the mixture of the ejecta and air, and (2) the turbulent mixing in and around the eruption clouds.

Previously, the dynamics of eruption cloud has been studied on the basis of steady one-dimensional (1-D) models [e.g., 2]. These models explain the fundamental features of eruption column (e.g., column height) and the condition for pyroclastic flow to generate; however, the phenomena which can be explained by these models are restricted to those of steady eruptions without any two-dimensional (2-D) or three-dimensional (3-D) effects (e.g., lateral spread of cloud and drift by wind). In order to explain time-dependent fluid dynamical features of explosive volcanism, several 2-D numerical models for eruption clouds have been developed over the past 20 years [3, 4]. These 2-D models reproduced the density change accompanied by turbulent mixing and explained the unsteady and multiphase features of eruption clouds. However, the features of turbulent mixing reproduced by these models were not quantitatively consistent with those observed in the laboratory experiments because of the low spatial resolution in their numerical simulations [5].

The aim of this paper is to develop a 3-D numerical model, which correctly reproduces both of the density change of the mixture of ejecta and air, and the quantitative features of turbulent mixing in and around eruption clouds. On the basis of the new model, the flow patterns near the vent are numerically simulated and some geological implications of the simulations are discussed.

2. Model Description

The numerical model of eruption cloud is based on the

* ***Corresponding author***: *Yujiro J. Suzuki, Institute for Research on Earth Evolution, Japan Agency for Marine-Earth Science and Technology, 3173-25, Showa-Machi, Yokohama 236-0001, Japan, E-mail: yujiros@jamstec.go.jp*

model of Suzuki et al. [5]. The model is designed to describe the injection of a mixture of pyroclasts and volcanic gas from a circular vent above a flat surface of the earth in a stationary atmosphere. In this paper, because we are particularly concerned with turbulent mixing of eruption clouds, we adopt a pseudo-gas model; we ignore the separation of pyroclasts from the eruption cloud, and the momentum and heat exchanges between the pyroclasts and gas are assumed to be so rapid that the velocity and temperature are the same for all the phases. These assumptions are valid when the size of pyroclasts is sufficiently small (< 4 mm) [6]. Sparks and Wilson [1] suggested that over 90% of the pyroclasts are less than 5 mm in diameter and over 60% are submillimeter in diameter for typical Plinian or phreatomagmatic eruptions. Pseudo-gas models are justified for such types of explosive eruptions.

The fluid dynamics model solves a set of partial differential equations describing the conservation of mass, momentum, and energy, and a set of constitutive equations describing the thermodynamic state of the mixture of pyroclasts, volcanic gas, and air. These equations are solved numerically by a general scheme for compressible flow with high spatial resolution. All the constants used in this study are listed in Table 1.

2.1 Governing Equations

The dynamics of eruption clouds is based on the Navier-Stokes equations of a compressible gas. Since the molecular viscosity is negligibly small compared to the eddy viscosity due to turbulence, we assume that the molecular viscosity is zero and that the equations are reduced to the Euler equation. The mass conservation for all the components (pyroclasts, volcanic gas, and air) is

$$\frac{\partial \rho}{\partial t} + \nabla \cdot (\rho \mathbf{u}) = 0, \tag{1}$$

where ρ is the density of the mixture, $\mathbf{u}$ is the velocity vector, and t is the time. The mass conservation equation for the ejecta from the vent is independently given as

$$\frac{\partial \rho \xi}{\partial t} + \nabla \cdot (\rho \xi \mathbf{u}) = 0, \tag{2}$$

where ξ is the mass fraction of the ejecta.

The conservation equations for momentum and energy are

$$\frac{\partial \rho \mathbf{u}}{\partial t} + \nabla \cdot (\rho \mathbf{u}\mathbf{u} + p\mathbf{I}) = \rho \mathbf{g}, \tag{3}$$

$$\frac{\partial \rho E}{\partial t} + \nabla \cdot [(\rho E + p)\mathbf{u}] = \rho \mathbf{g} \cdot \mathbf{u}, \tag{4}$$

where p is the pressure, $\mathbf{I}$ is the unit matrix, $\mathbf{g}$ is the gravitational body force per unit mass, and E is the total energy per unit mass, that is, the internal energy (e) plus kinetic energy (K): $E = e + K$.

2.2 Constitutive Equation

On the assumption that the differences of velocity and temperature between pyroclasts and gas are zero, the equation of state for the mixture of the ejecta and air is

$$\frac{1}{\rho} = \frac{n_s}{\sigma} + \frac{(n_g R_g + n_a R_a)T}{p}, \tag{5}$$

where σ is the density of the pyroclasts, R_g and R_a are the gas constants of volcanic gas and air, respectively, and T is the temperature. The mass fractions of pyroclasts (n_s), volcanic gas (n_g), and air (n_a) satisfy the condition of $n_s + n_g + n_a = 1$. The mass fraction of the ejecta in the eruption cloud is given by $\xi = n_s + n_g$. The initial mass fraction of volcanic gas (i.e., volatile content in the magma) is given by $n_{g0} = n_g/(n_s + n_g)$ using these nota-

Table 1 List of Material Properties and Values of Physical Parameters.

Variable	Value	Units	Meaning
g	9.81	m s^{-2}	gravitational body force
R_g	462	J $kg^{-1}K^{-1}$	gas constant of volcanic gas
R_a	287	J $kg^{-1}K^{-1}$	gas constant of atmospheric air
C_{vs}	1100	J $kg^{-1}K^{-1}$	specific heat of pyroclasts
C_{vg}	1155	J $kg^{-1}K^{-1}$	specific heat of volcanic gas at constant volume
C_{va}	713	J $kg^{-1}K^{-1}$	specific heat of atmospheric air at constant volume
γ	1.402	-	ratio of specific heat for gas phase
T_{a0}	303	K	temperature of air at z = 0 km
p_{a0}	1.013x10^5	Pa	pressure of air at z = 0 km
ρ_{a0}	1.13	kg m^{-3}	density of air at z = 0 km

tions. The subscripts s, g and a refer to pyroclasts, volcanic gas and air, respectively.

The change of internal energy is proportional to the change of temperature:

$$de = C_{\mathrm{vm}} dT, \tag{6}$$

where C_{vm} is the average specific heat at constant volume, which is defined using the specific heats of pyroclasts (C_{vs}), volcanic gas (C_{vg}), and air (C_{va}) as

$$C_{\mathrm{vm}} = n_{\mathrm{a}} C_{\mathrm{va}} + n_{\mathrm{g}} C_{\mathrm{vg}} + n_{\mathrm{s}} C_{\mathrm{vs}}. \tag{7}$$

The subscript m in C_{vm} refers to the mixture of the ejecta (i.e., pyroclasts and volcanic gas) and entrained air. When the specific heats of each component (C_{vs}, C_{vg}, and C_{va}) are constant, we can define the internal energy of the mixture, e, in the equation of energy conservation (Eq.4) such that

$$e = C_{\mathrm{vm}} T, \tag{8}$$

without loss of generality.

2.3 Boundary Conditions

The physical domain involves a horizontal and vertical extent of more than several tens of kilometers. We carried out the simulations in 2-D and 3-D coordinates for comparison. In the 2-D model, the vent is located in the lower left-hand corner of the computational domain, in which the pressure, exit velocity, mass fraction of volcanic gas, temperature, and density are fixed and constant. The axis of the flow is modeled as a free-slip reflector in order to preserve the symmetry of the system in the 2-D model. In the 3-D model, in contrast, the vent is located in the center of the ground surface, and no boundary condition along the central axis of the flow is required. At the ground boundary, the free-slip condition is assumed for the velocity of the ejected material and air. At the upper and other edges of computational domain, the fluxes of mass, momentum, and energy are assumed to be continuous, and these boundary conditions correspond to free outflow and inflow of these quantities.

We assume that the pressure at the vent (p_0) is equal to the atmospheric pressure at z = 0 km (p_{a0}), and that the exit velocity (u_0) is larger than the sound velocity of the ejecta. When the initial mass fraction of volcanic gas (n_{g0}), magmatic temperature (T_0), and p_0 are given, the density of the ejecta (ρ_0) is calculated from the equation of state (Eq.5). When the vent radius (L_0) and u_0 are specified as parameters, the mass discharge rate is calculated from the relationship as

$$\dot{m}_0 = \rho_0 u_0 (\pi L_0^2). \tag{9}$$

2.4 Numerical Procedure

The partial differential equations (Eqs.1, 2, 3, and 4) are solved numerically for ρ, $\rho\mathbf{u}$, ρE, and $\rho\xi$ by the Roe scheme [7] in space, which is a general total variation diminishing (TVD) scheme for compressible flow and can simulate a generation of shock waves inside and around the high-speed jet correctly. The MUSCL method [8] is applied to interpolate the fluxes between grid points, and therefore our numerical model achieves third-order accuracy in space. These equations are solved using the time splitting method. We treat the gravitation term of the equations of momentum and energy conservation (Eqs.3 and 4), and the additional terms due to the curvature of axisymmetric 2-D coordinates as source terms. The density, velocity, total energy, and the mass fraction of the ejecta are solved fully explicitly. The present numerical code is based on the astronomical work of Hachisu et al. [9], who reproduced most of the observational indications of mixing in SuperNova 1987A.

3. Density Change of Ejecta and Air Mixture

The density of the mixture of the ejecta and air at constant pressure as a function of the mass fraction of the ejecta can be analytically derived. When the ejecta with a high temperature, T_0, and air with a low temperature, T_{a}, are mixed and reach thermal equilibrium at a constant pressure, p, the equilibrium temperature for the mixture, T_{m}, has the form

$$T_{\mathrm{m}} = \frac{\xi C_{\mathrm{p0}} T_0 + (1-\xi) C_{\mathrm{pa}} T_{\mathrm{a}}}{\xi C_{\mathrm{p0}} + (1-\xi) C_{\mathrm{pa}}}, \tag{10}$$

where C_{p0} and C_{pa} are the specific heat of the ejecta and air at constant pressure, respectively. At the same time, this new mixture satisfies the equation of state as

$$p = \frac{\rho [\xi n_{\mathrm{g0}} R_{\mathrm{g}} + (1-\xi) n_{\mathrm{a}} R_{\mathrm{a}}] T_{\mathrm{m}}}{(1-A)}, \tag{11}$$

where A is the volume fraction of the solid in the eruption cloud: $A = \rho\xi n_{\mathrm{s0}}/\sigma$ (<< 1). Combining Eqs.10 and 11 and using the equation of state for air ($p = \rho_{\mathrm{a}} R_{\mathrm{a}} T_{\mathrm{a}}$), the mixture density relative to air is obtained as

$$\frac{\rho}{\rho_{\mathrm{a}}} = \frac{R_{\mathrm{a}} (1-A)}{\xi n_{\mathrm{g0}} R_{\mathrm{g}} + (1-\xi) n_{\mathrm{a}} R_{\mathrm{a}}} \frac{\xi C_{\mathrm{p0}} + (1-\xi) C_{\mathrm{pa}}}{\xi C_{\mathrm{p0}} T_0 + (1-\xi) C_{\mathrm{pa}} T_{\mathrm{a}}} T_{\mathrm{a}}. \tag{12}$$

Fig. 1 illustrates the density change of the mixture on the basis of Eq.12. The ejecta have an initial density of

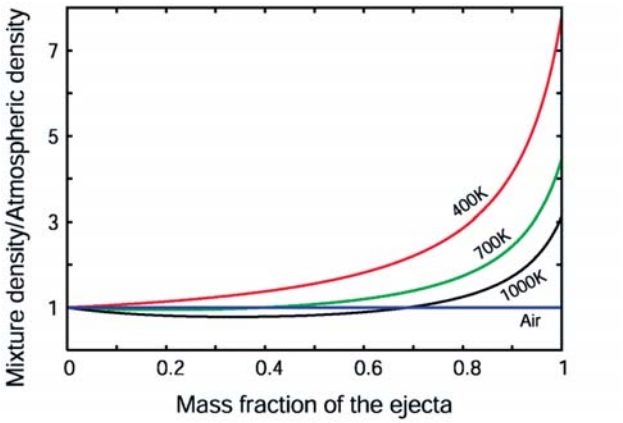

Fig. 1 Variation of the mixture density of the ejecta plus ambient air as a function of the mass fraction of the ejecta in the mixture. The density is normalized by the atmospheric density. Curves are shown for an initial mass fraction of volcanic gas of 0.06 with an initial temperature of 400 K (red curve), 700 K (green curve), and 1000 K (black curve). The temperature of atmospheric air is set to be 303 K.

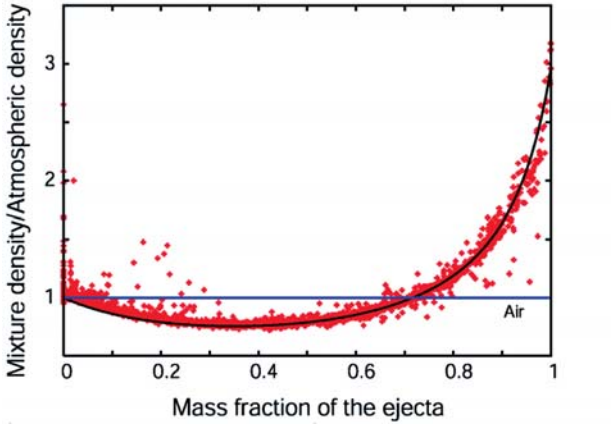

Fig. 2 The mixture density of the ejecta plus ambient air as a function of the mass fraction of the ejecta in the mixture. Red plots are the mixture density on all the grids in the 3-D simulation. Black curve is the mixture density on the basis of Eq.12. The density is normalized by the atmospheric density. The initial temperature and the initial mass fraction of volcanic gas in the ejecta at the vent are assumed to be T_0 = 1053 K and n_{g0} = 0.06, respectively. The temperature of atmospheric air is set to be 303 K.

several times as large as the atmospheric density. As the ejected material is mixed with ambient air and the mass fraction of the ejecta decreases, the density of the mixture drastically decreases and becomes less than the atmospheric density. The density of the mixture is also a function of magmatic temperature. As the magmatic temperature decreases, the critical mass fraction at which the density of the mixture is equal to that of air decreases. In the case that the magmatic temperature is less than 400 K, the mixture is always heavier than air. Such situations may be relevant to phreatomagmatic eruptions [e.g., 10]. It must be noted that the density of the mixture is also a function of the initial mass fraction of volcanic gas, n_{g0}.

We reproduce the nonlinear features of the density change of the mixture of the eruption cloud and air in Fig. 1 by changing the effective gas constant of the mixture in the equation of state for ideal gases. The first term of the right-hand side of Eq.5 represents the volume of the solid phase in a unit mass of the mixture, and the second term represents the volume of the gas phase. The first term is negligible relative to the second term when the pressure is close to atmospheric pressure (10^5 Pa), because the density of the pyroclasts is 10^3 times as large as that of the gas phase. Therefore Eq.5 can be approximated by the equation of state for an ideal gas as

$$p \approx \rho (n_g R_g + n_a R_a) T \equiv \rho R_m T, \tag{13}$$

where R_m is the average gas constant. Since the ratio of specific heat at constant volume and constant pressure of the mixture can be defined as

$$\gamma_m \equiv 1 + \frac{R_m}{C_{vm}}, \tag{14}$$

we can calculate the pressure at the position with an arbitrary mixing ratio using Eqs.8, 13, and 14 as

$$p = (\gamma_m - 1)\rho e. \tag{15}$$

On the above assumption of the equation of state (i.e., Eq.13), we derive analytically the eigenvalues and eigenvectors for the governing equations of two fluids (i.e., the ejecta and air) [11], and apply the Roe scheme to the present problem of the dynamics of eruption clouds. After the density, velocity, total energy, and the mass fraction of the ejecta are calculated using Eqs.1, 2, 3, and 4, the temperature and pressure are updated employing Eqs.8 and 15, respectively.

We compare the density change reproduced by the 3-D numerical model with that analytically derived from Eq.12 (Fig. 2). In this simulation it is assumed that the mixture of hot pyroclasts and volcanic gas is ejected into a uniform air. Our simulation has successfully reproduced the nonlinear feature of equation of state.

4. Turbulent Mixing

The efficiency of turbulent mixing, in general, is a function of the Reynolds number [12]. At $Re < 10^4$, even though the flow may be unsteady, the efficiency of mixing increases with *Re*, and the resulting turbulent flow

cannot be described as fully developed. On the other hand, at $Re > 10^4$ the efficiency of entrainment no longer depend on Re, and the turbulence is fully developed. We call this transition to the fully turbulent flow ($Re \sim 10^4$) "mixing transition". Because the flow of eruption clouds is considered to be fully turbulent, the simulations of eruption clouds should be carried out above the mixing transition ($Re > 10^4$).

A number of theoretical and experimental studies on a fully-developed turbulent jet or plume which is ejected from a nozzle into a uniform environment (refereed to as "JPUE") have revealed that such a JPUE is characterized by the self-similarity that the radial length scale is proportional to the distance from the nozzle (or a virtual point of origin). This means that the evolution of the JPUE is determined solely by the local scales of length and velocity [13]. Experimental studies have also shown that the time-averaged horizontal profile of jet can be approximated by the Gaussian profile and its width represents the efficiency of entrainment.

The above features of JPUE result from the two processes of turbulent mixing: (1) engulfment process [14] and (2) diastrophy and infusion processes [15]. The engulfment of ambient fluid is caused by the large-scale structures of turbulence. Subsequently, turbulent straining of the entrained fluid reduces its spatial scale to a small enough value at which viscous diffusion dominates (diastrophy). Finally, because of viscous diffusion, the inducted fluid is mixed at the molecular level with the turbulent flow (infusion). The global features of turbulent mixing above the mixing transition such as a self-similarity are mainly controlled by the engulfment process. The diastrophy and infusion processes are associated with smaller-scale vortices than those of the engulfment process. In order to reproduce these processes of turbulent mixing numerically, we consider two factors of numerical procedure: (1) three dimensionality and (2) spatial resolution. Since the large-scale structures of turbulence are 3-D in general, the engulfment process should be reproduced on 3-D coordinates. In addition, the grid size should be small enough to resolve the large-scale structures of the engulfment process [16].

In the following, we systematically evaluate the effects of the above two factors on the entrainment process. For this purpose, we carried out simulations for the case of the JPUE, whose qualitative and quantitative features were experimentally investigated by a number of previous workers [e.g., 17]. In these simulations, it is assumed that both the ejected and surrounding fluids are air with the same temperature (T = 273 K) and the same ratio of specific heat ($\gamma = 1.40$). The numerical conditions for the simulations of JPUE (e.g., grid size and number of grid points) are summarized in Table 2.

Table 2 Numerical Conditions of the Simulations of Turbulent Jets.

	Dimensions	Accuracy of scheme	Δx	Number of grid points
Run J1	3-D	3rd	$L_0/5$	384x384x512
Run J2	2-D	3rd	$L_0/5$	384x512
Run J3	3-D	1st	$L_0/5$	384x384x512
Run J4	3-D	3rd	$L_0/1$	80x 80x128
Run J5	3-D	3rd	$L_0/2$	160x160x224
Run J6	3-D	3rd	$L_0/3$	192x192x256
Run J7	3-D	3rd	$L_0/4$	384x384x512
Run J8	3-D	3rd	$L_0/8$	506x506x1012

4.1 Effects of Three Dimensionality

We simulate the turbulent jet with axisymmetric 2-D and 3-D coordinates and compare our results with the experimental studies from the viewpoint of self-similarity. In the 3-D simulations, the ejected fluid exhibits a meandering instability where the axis of the flow varies with height, which causes efficient turbulent mixing of the ejected and surrounding fluids (Fig. 3a). As a result, the radius of jet increases linearly with height. These features are consistent with the laboratory experiments [17]. On the other hand, in the axisymmetric 2-D simulations, the ejected fluid rises along the central axis and the spreading rate of the jet is substantially smaller than the results of the 3-D simulations (Figs. 3b and 4). This difference implies that the efficiency of turbulent mixing is significantly reduced because of the boundary condition at the centerline of the axisymmetric coordinates and underpins the significance of the 3-D coordinates for the simulation of turbulent mixing.

4.2 Effects of Spatial Resolution

High spatial resolution can be attained by (1) high-order accuracy schemes and (2) fine grid sizes. We evaluate these two effects here. Fig. 3a indicates that the third-order accuracy scheme with a fine grid size reproduces the turbulence containing the various scale of vortices, which causes efficient turbulent mixing of the ejected and surrounding fluids. On the other hand, in the simulations of the first-order accuracy scheme with the same grid size (Fig. 3c) or those of the third-order accuracy scheme with a coarse grid size (Fig. 3d), the vortical structures of the JPUE are not correctly reproduced. In these simulations, the spreading rate of the jet is smaller than that of the 3-D simulation using the third-order accuracy scheme with a fine grid size, suggesting that the efficiency of entrainment is substantially reduced in these simulations (Fig. 4).

We also compare our results with the experimental

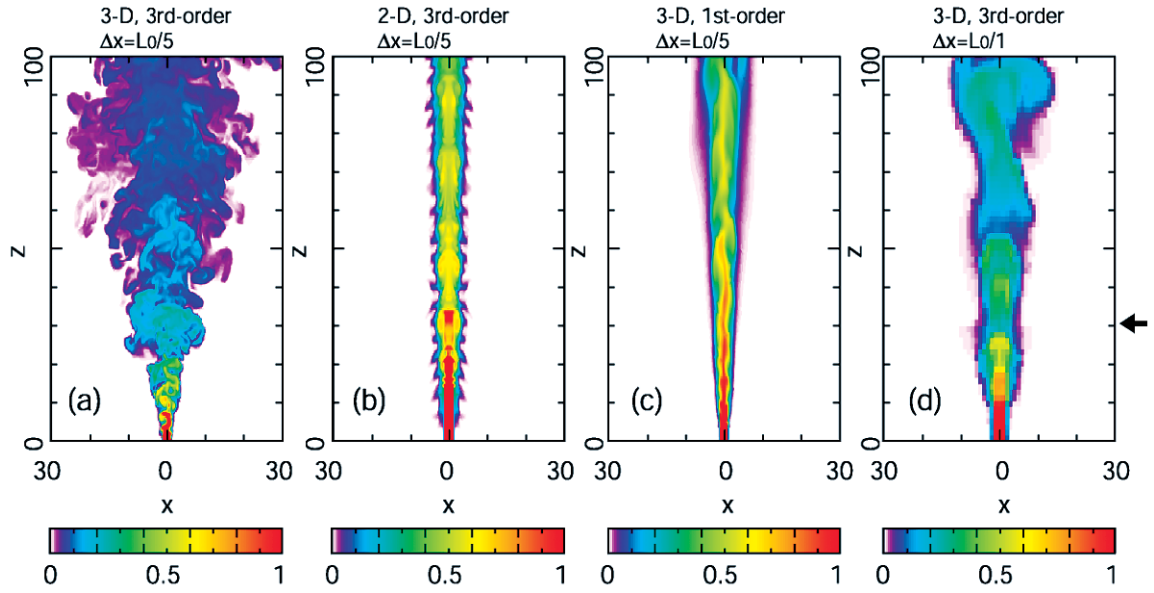

Fig. 3 Numerical results of turbulent jets ejected into the same fluid. The color illustrates the cross-sectional distribution of the mass fraction of the ejected fluid. The horizontal distance from the centerline and the vertical distance from the nozzle are represented by x and z, respectively. (a) Simulation of the third-order accuracy scheme with $\Delta x = L_0/5$ in 3-D coordinates where Δx is the grid size, L_0 is the nozzle radius. (b) Simulation of the third-order accuracy scheme with $\Delta x = L_0/5$ in 2-D coordinates. (c) Simulation of the first-order accuracy scheme with $\Delta x = L_0/5$ in 3-D coordinates. (d) Simulation of the third-order accuracy scheme with $\Delta x = L_0/1$ in 3-D coordinates.

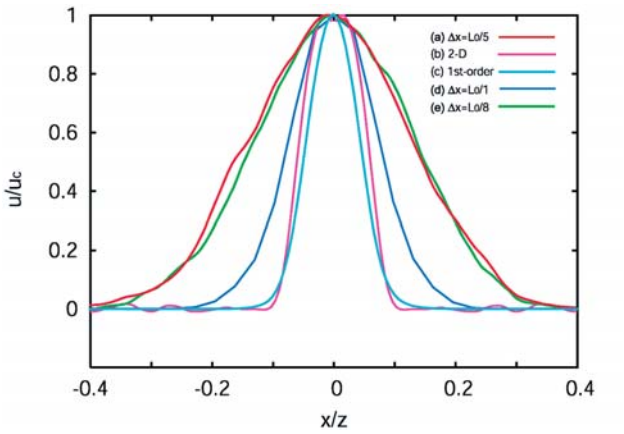

Fig. 4 Velocity profiles across a turbulent jet. Vertical axis represents the vertical velocity normalized by the centerline value (u_c). Horizontal axis represents dimensionless displacement (x/z). Curves a, b, c, and d are the time- averaged velocity profiles at fixed cross sections for the simulations of Fig. 3a, 3b, 3c, and 3d, respectively. The heights of the cross sections are shown by arrows in Fig. 3 (z = 30 m). Curve e illustrates the simulation of the third-order accuracy scheme in 3-D coordinates with $\Delta x = L_0/8$.

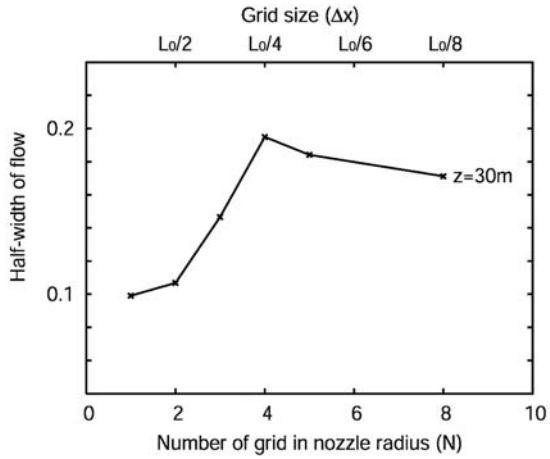

Fig. 5 Half-width of flow as a function of the number of grid points in nozzle radius when the vertical profile is approximated by the Gaussian profile. The heights of the cross sections are shown by arrows in Fig. 3 (z = 30 m).

studies from the viewpoint of the dependency of the efficiency of mixing on "the numerical Reynolds number" (Re*). In a numerical simulation of fluid dynamics, Re* increases with increasing spatial resolution. On the other hand, the width of jet represents the efficiency of mixing. Therefore, we investigate the dependency of the width of jet on the grid size (or the number of grid in nozzle radius) (Fig. 5). The normalized width of flow increases as the number of grid (N) increases when N is less than 4, and asymptotically approaches a constant value when N is more than 4. These results are consistent with the general feature of turbulent mixing reported by the experimental studies. It is suggested that the condition above the mixing transition is achieved when $N > 4$.

4.3 Summary of Treatment for the Turbulent Mixing

According to the previous experimental studies of JPUE, the key step in the entrainment process during turbulent mixing is the one that controls the rate at which ambient fluid enters into the turbulent region, i.e., the engulfment process [18]. Judging from the numerical simulations for the JPUE, it is essential to apply 3-D coordinates with a sufficiently high spatial resolution in order to correctly reproduce the engulfment process; simulations should be carried out above the mixing transition where the efficiency of entrainment is independent of Re^* (i.e., independent of grid sizes).

5. Turbulent Mixing in Eruption Clouds

Turbulent jets and plumes of eruption clouds differ in several ways from the ideal situations of the JPUE. In eruption clouds the magnitude of buoyancy drastically changes with the amount of entrained air due to the nonlinear feature of the equation of state (Fig. 1), whereas the relationship between ρ and ξ can be approximated by a linear function in the case of the JPUE. Secondly, the surrounding atmosphere is not uniform but stratified. Thirdly, the length scale of source (i.e., crater size) cannot be ignored near the vent in comparison with the downstream distance from the vent in the natural volcanic system. Because of these differences, the assumption of self-similarity is not necessarily valid for the flow of eruption clouds. In the preceding section we have developed a numerical model which can reproduce the general features of turbulent mixing in the JPUE. We perform the numerical simulations for the actual conditions of explosive eruptions into a stratified environment, and systematically investigate how the features of turbulent mixing and the flow patterns are modified.

Our simulations have reproduced the behavior of eruption clouds including eruption columns and/or the formation of pyroclastic flows and the unsteady and multidimensional features of eruption clouds. Table 3 lists the initial conditions and numerical conditions for the simulations. In Runs 1, 2, and 3, an initial temperature of T_0 = 1000 K and initial mass fraction of volcanic gas of n_{g0} = 0.05 are assumed. We increase vent radius from 69 to 613 m and see how the flow patterns change in these runs. In Run 4, we use a lower temperature condition (T_0 = 400 K, n_{g0} = 0.10) with a small vent radius (20 m) for comparison. Following the results of simulations of turbulent jets (section 4), Δx is set to be $L_0/5$ (see Table 3 for the grid sizes and the number of grid points). We use 512 processors (i.e., 64 nodes) of the Earth Simulator with 640 gigabyte of memory.

In the case that the vent radius is small (69 m in Run 1), a stable eruption column forms; the eruption cloud becomes buoyant before the initial momentum at the vent is exhausted (Fig. 6a). The flow is characterized by a concentric structure consisting of an outer shear region and inner dense core. In the outer shear region, the ejecta and ambient air are efficiently mixed by the eddy due to shear so that the density of the mixture becomes less than that of air. In the inner dense core, the ejecta are not mixed with ambient air. As the eruption cloud ascends, the inner dense core disperses because of erosion by the outer shear region; the eruption column rises as a fully turbulent plume.

In the case that the vent radius is large (218 m in Run 2), the outer shear region cannot reach the central axis before the initial momentum is exhausted (Fig. 6b). The inner dense core is maintained up to a height of 2 km and the top of the inner dense core subsequently spreads radially. This structure is called as "the radially suspended flow". Then inner dense core and outer shear region are mixed by the large-scale eddy of the suspended flow. Consequently, the resultant mixture becomes buoyant and produces another type of stable column.

When the vent radius is extremely large (613 m in Run 3), the eruption column collapses to spread radially as a pyroclastic flow (Fig. 6c). Only a small amount of air is entrained into the eruption cloud in the case of large vent radius, so that, the most parts of the mixture due to the suspended flow remain heavier than air and collapses to the ground. The upper region of the pyroclastic flow entrains air and forms buoyant co-ignimbrite ash clouds.

When the initial temperature is low and the vent radius is small (Run 4 with T_0 = 400 K and L_0 = 20 m; Fig. 6d),

Table 3 Input Parameters and Numerical Conditions of the Simulations of Eruption Clouds.

	T_0 [K]	L_0 [m]	m_0 [kg s^{-1}]	u_0 [m s^{-1}]	Δx [m]	Number of grid points
Run 1	1000	69	10^7	154	13	512x512x512
Run 2	1000	218	10^8	154	44	512x512x512
Run 3	1000	613	$10^{8.9}$	154	123	512x512x512
Run 4	400	20	10^6	139	4	512x512x512

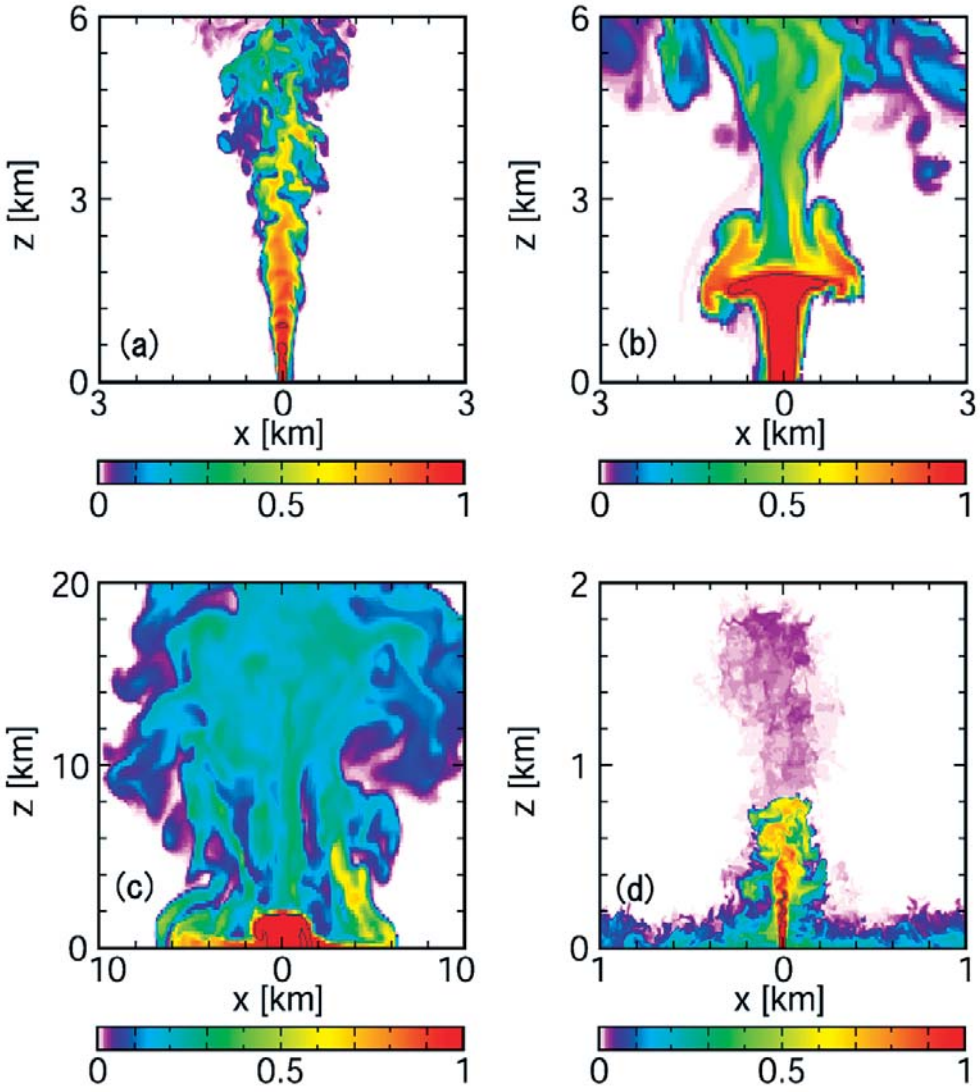

Fig. 6 Representative numerical results of (a) stable column regime (Run 1), (b) stable column regime which is characterized by the suspended flow of the inner dense core (Run 2), (c) column collapse regime which is characterized by the suspended flow (Run 3), and (d) column collapse regime (Run 4). Parameters used and conditions at the vent are listed in Tables 1 and 2. Cross-sectional distributions of the mass fraction of the ejecta ξ are shown in *x*-*z* space. The contour levels in plots are $\xi = 0.97$. We call the region where the mass fraction of the ejecta is 1.0 the inner dense core. It is surrounded by the outer shear region, where the ejecta entrain ambient air.

the column collapse occurs without inner dense core developing a suspended flow; collapse occurs after the inner dense core disperses because of erosion by the outer shear region. Although a jet with a small vent radius efficiently entrains ambient air before the initial momentum is exhausted, the mixture of the ejecta and air is always heavier than air when T_0 is as low as 400 K (Fig. 1). As a result, all the eruption cloud collapses to the ground and cannot generate a co-ignimbrite ash cloud from a pyroclastic flow [cf. 10].

As described above, the flow pattern of eruption cloud varies depending on the vent radius. A column with a small vent radius behaves as a typical turbulent plume and approximately attains the self-similarity. On the other hand, when the vent radius is large, eruption clouds shows multi-dimensional features and the self-similarity is not attained.

In the case of JPUE, it is essential to apply 3-D coordinates in order to correctly reproduce the self-similarity observed in laboratory experiments (see Section 4). We also simulate the eruption cloud for the same condition as Run 1 with axisymmetric 2-D coordinates and investigate the effects of three-dimensionality on the dynamics of eruption clouds. In the 3-D simulation, the radius of flow

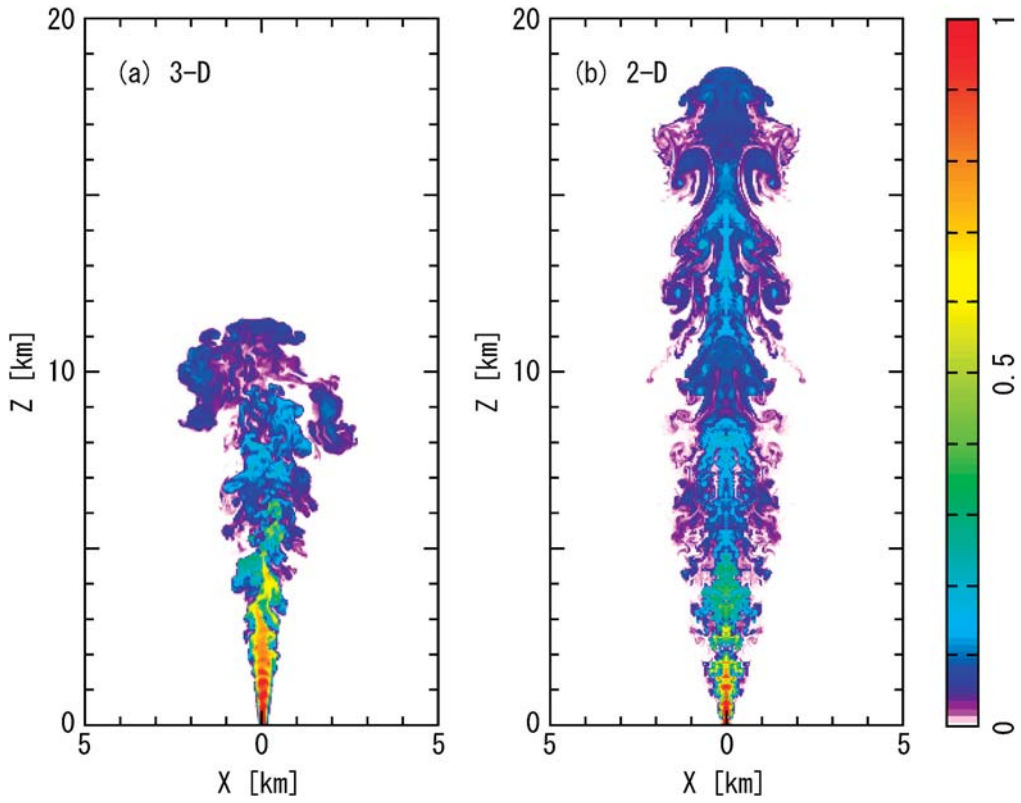

Fig. 7 Numerical results of eruption clouds at 200 s from the beginning of eruption in Run 1. (a) Simulation of 3-D coordinates. (b) Simulation of axisymmetric 2-D coordinates. The color illustrates the cross-sectional distribution of the mass fraction of the ejecta (pyroclasts plus volcanic gas). Parameters used and conditions at the vent are listed in Tables 1 and 2.

increases linearly with height as a result of the efficient mixing by the meandering instability (Fig. 7a). On the other hand, in the axisymmetric 2-D simulations, the ejecta rise along the central axis and the column is substantially higher than the results of the 3-D simulations (Fig. 7b). This difference implies that the efficiency of turbulent mixing is significantly reduced because of the boundary condition at the centerline of the axisymmetric coordinates and that the three-dimensionality plays an important role in simulating the dynamics of eruption clouds such as column heights.

6. Geological Implications

The dynamics of eruption clouds are governed by turbulent mixing between eruption clouds and ambient air and the density change of eruption clouds accompanied by turbulent mixing. Previously, the fluid dynamics and the thermodynamics of eruption clouds have been studied on the basis of steady one-dimensional (1-D) models [e.g., 2]. In the steady 1-D models, turbulent mixing between eruption clouds and ambient air are modeled by the entrainment hypothesis that the mean inflow velocity across the edge of turbulent flow (jet and/or plume) is proportional to the mean vertical velocity; the proportionality constant (i.e., entrainment coefficient) represents the efficiency of turbulent mixing. The entrainment hypothesis is supported by the laboratory experiments where the diameter of turbulent jet injected into a uniform environment linearly increases with the distance from the source. The steady 1-D models using the entrainment coefficient based on those laboratory experiments have accounted for fundamental features of a steady state of eruption clouds and the critical conditions for column collapse. However, these results of the steady 1-D models largely depend on the assumed value of entrainment coefficient. Besides, the steady 1-D models could not describe unsteady and multi-dimensional features of actual eruption clouds.

In the present study, we have developed a 3-D fluid dynamics model which simulates turbulent mixing in and around eruption clouds without any a priori assumptions. Our model reproduces the quantitative features of turbulent jets and plumes observed in the laboratory experiments, and it has also successfully reproduced the basic features of eruption clouds such as generation of eruption columns and column collapse. In addition, it has reproduced unsteady and multi-dimensional features of erup-

tion clouds such as a suspended flow and pyroclastic flow.

Our model is expected to be useful for volcanological problems in several ways. First, we can systematically investigate unsteady and multi-dimensional fluid dynamical phenomena observed in actual volcanic eruptions. For example we can simulate the dynamics of large-scale umbrella clouds which are directly observed in satellite images during explosive eruptions by using 1600 processors (i.e., 200 nodes) of the Earth Simulator with 1 terabyte of memory for 12.3 billion grid points (2040 × 2040 × 506 grid points). Our model would also be useful to improve the quality of existing 1-D steady models which can run standard personal computers. Through the comparisons between the results of our 3-D simulations and those of the steady 1-D models, we can propose preferable values of the entrainment coefficient to predict eruption column dynamics correctly during steady explosive eruptions.

Acknowledgements

Numerical computations were in part carried out on the Earth Simulator at Japan Agency for Marine-Earth Science and Technology. Part of this study was supported by funds from Ministry of Education, Culture, Sports, Science and Technology (Nos.18340130 and 18710154).

(This article is reviewed by Dr. Yozo Hamano.)

References

[1] R. S. J. Sparks, and L. Wilson, A model for the formation of ignimbrite by gravitational collapse, *J. Geol. Soc. London*, vol.**132**, pp.441–452, 1976.

[2] A. W. Woods, The fluid dynamics and thermodynamics of eruption columns, *Bull. Volcanol.*, vol.**50**, pp.169–193, 1988.

[3] K. H. Wohletz, T. R. McGetchin, M. T. Sandford II, and E. M. Jones, Hydrodynamic aspects of caldera-forming eruptions: Numerical models, *J. Geohys. Res.*, vol.**89**, no.B10, pp.8269–8285, 1984.

[4] A. Neri, T. E. Ongaro, G. Macedonio, and D. Gidaspow, Multi-particle simulation of collapsing volcanic columns and pyroclastic flow, *J. Geophys. Res.*, vol.**108**, no.B4, 2202, doi:10.1029/2001JB000508, 2003.

[5] Y. J. Suzuki, T. Koyaguchi, M. Ogawa, and I. Hachisu, A numerical study of turbulent mixing in eruption clouds using a three-dimensional fluid dynamics model, *J. Geophys. Res.*, vol.**110**, B08201, 2005.

[6] A. W. Woods, and M. I. Bursik, Particle fallout, thermal disequilibrium and volcanic plumes, *Bull. Volcanol.*, vol.**53**, pp.559–570, 1991.

[7] P. L. Roe, Approximate Riemann solvers, parameter vectors, and difference schemes, *J. Comput. Phys.*, vol.**43**, pp.357–372, 1981.

[8] B. van Leer, Towards the ultimate conservative difference scheme III. Upstream-centered finite-difference scheme for ideal compressible flow, *J. Comput. Phys.*, vol.**23**, pp.263–275, 1977.

[9] I. Hachisu, T. Tatsuda, K. Nomoto, and T. Shigeyama, Nonlinear growth of Rayleigh-Taylor instabilities and mixing in SN 1987A, *Astrophys. J.*, vol.**358**, pp.57–61, 1990.

[10] T. Koyaguchi, and A. Woods, On the formation of eruption columns following explosive mixing of magma and surface-water, *J. Geophys. Res.*, vol.**101**, no.B3, pp.5561–5574, 1996.

[11] Y. Wada, H. Kubota, T. Ishiguro, and S. Ogawa, A fully implicit high-resolution scheme for compressible chemically reacting flows, in *Nonlinear Hyperbolic Equations: Theory, Computation Methods, and Applications: Proceedings of the Second International Conference on Nonlinear Hyperbolic Problems, Notes Numer. Fluid Mech.*, vol.**24**, ed. J. Ballmann, and R. Jeltsch, pp.648–659, F. Vieweg, Wiesbaden, Germany, 1989.

[12] P. E. Dimotakis, and H. J. Catrakis, Turbulence, Fractals, and Mixing in *Mixing*: *Chaos and Turbulence*, *NATO ASI Ser., Ser. B, Phys.*, ed. H. Chate, E. Villermaux, and J. M. Chomaz, vol.**373**, pp.59–143, Plenum Pub Corp, New York, 1999.

[13] H. Tennekes, and J. L. Lumley, *A first Course in Turbulence*, pp.300, MIT Press, Cambridge, Mass, 1972.

[14] J. Mathew, and A. J. Basu, Some characteristics of entrainment at a cylindrical turbulence boundary, *Phys. Fluids*, vol.**14**, pp.2065–2072, 2002.

[15] P. E. Dimotakis, Two-dimensional shear-layer entrainment, *AIAA J.*, vol.**24**, pp.1791–1796, 1986.

[16] P. Moin, and J. Kim, Numerical investigation of turbulent channel flow, *J. Fluid Mech.*, vol.**118**, pp.341–377, 1982.

[17] H. B. Fisher, E. J. List, R. C. Y. Koh, J. Imberger, and N. H. Brooks, *Mixing in Inland and Coastal Waters*, pp.483, Elsevier, New York, 1979.

[18] J. S. Turner, Turbulent entrainment: The development of the entrainment assumption, and its application to geological flows, *J. Fluid Mech.*, vol.**173**, pp.431–471, 1986.